

A microelectromechanical load sensor for *in situ* electron and x-ray microscopy tensile testing of nanostructures

Yong Zhu, N. Moldovan, and Horacio D. Espinosa^{a)}

Department of Mechanical Engineering, Northwestern University, 2145 Sheridan Road, Evanston, Illinois 60208

(Received 4 August 2004; accepted 3 November 2004; published online 28 December 2004)

We report on the performance of a microelectromechanical system (MEMS) designed for the *in situ* electron and x-ray microscopy tensile testing of nanostructures, e.g., carbon nanotubes and nanowires. The device consists of an actuator and a load sensor with a gap in between, across which nanostructures can be placed, nanowelded, and mechanically tested. The load sensor is based on differential capacitance measurements, from which its displacement history is recorded. By determining the sensor stiffness, the load history during the testing is obtained. We calibrated the device and examined its resolution in the context of various applications of interest. The device is the first true MEMS in which the load is electronically measured. It is designed to be placed in scanning and transmission electron microscopes and on x-ray synchrotron stages. © 2005 American Institute of Physics. [DOI: 10.1063/1.1844594]

Advances in nanotechnology require the development of experimental techniques capable of measuring mechanical properties of nanostructures, such as carbon nanotubes (CNTs), nanowires (NWs), and ultrathin films. While challenging, a variety of experimental techniques dedicated to this purpose have been developed in the past decade including resonance test,^{1,2} bending test,^{3,4} and tensile test.^{5–8}

Tensile testing is the most widely used technique in macro- and microscale material characterization. In the testing of nanostructures, measuring load—displacement signatures is a major challenge. Though ingenious experiments have been carried out,^{5,7} a major limitation to date is that both deformation and load are deduced from the microscopic imaging of the specimen and testing apparatus. The limitation arises from the fact that both specimen deformation and load sensor displacement need to be imaged. When high magnifications are employed or in x-ray setups, these two measurements cannot be made simultaneously. In the case of electron microscopy a shift of the beam between specimen and load sensor is required.

Here we report a microelectromechanical system (MEMS) designed for the tensile testing of nanostructures using an alternative approach, which is to measure the load electronically. This scheme leaves open the possibility of *continuous* observation of the specimen deformation and failure at high magnification, while independently measuring the applied load. Due to its small size, the MEMS is well suited for *in situ* testing of NWs, CNTs and electron transparent films inside scanning electron microscope (SEM), transmission electron microscope (TEM), and on x-ray synchrotron stages.

The device consists of three parts: actuator, load sensor, and a gap for placement of nanostructures, as shown in Figs. 1(a) and 1(b). The devices were fabricated at MEMSCAP (Durham, NC) using the Multi User MEMS Process (MUMPs). Two types of actuators, a thermal actuator⁹ and an electrostatic (comb drive) actuator¹⁰ were designed. Due

to the large stiffness of the thermal actuator, it works in a displacement-controlled fashion. By contrast, the comb drive actuator is force controlled. The thermal actuator has the capability of testing stiffer structures, e.g., nanoscale thin films and large diameter NWs, while the comb drive actuator is suited for relatively compliant structures, e.g., CNTs and small diameter NWs.

The load sensor incorporated in the testing apparatus is based on differential capacitive sensing.^{11–13} The sensor displacement is determined by the measured capacitance change. Its stiffness is optimized to achieve maximum displacement at the specimen failure load. By knowing the sensor stiffness from mechanical resonance experiments,¹⁰ the load (force)—capacitance change relationship can be obtained. The key of the load sensor is to measure displacement in terms of capacitance change with high resolution.

The differential capacitive sensor consists of a rigid shuttle with one set of movable electrodes (beams) and two sets of stationary electrodes (beams). Each movable beam is initially equally spaced between two stationary beams. The

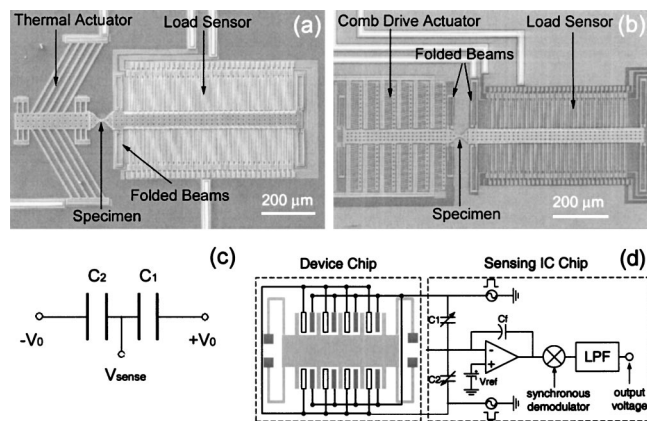


FIG. 1. (a) *In situ* tensile testing device including thermal actuator, load sensor, and specimen; (b) device including comb drive actuator, load sensor, and specimen; (c) circuit model for the load sensor; (d) schematic of the double chip scheme (device chip and sensing IC chip) used to measure the capacitance change.

^{a)} Author to whom correspondence should be addressed; electronic mail: espinosa@northwestern.edu

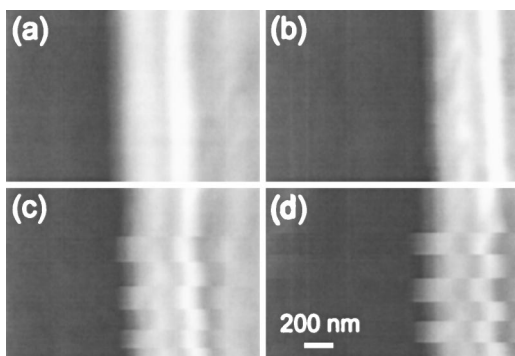


FIG. 2. SEM images at (a) 1 V, (b) 2.5 V, (c) 4 V, and (d) 5.5 V actuation voltages. During the image scanning, the device actuation was turned ON and OFF for 6 times. The scale bar is the same for all images.

entire capacitance sensor is equivalent to two capacitors with capacitances of C_1 and C_2 , as shown in Fig. 1(c), namely,

$$C_1 = C_2 = C_0 = \epsilon N \frac{A}{d_0} (1 + f), \tag{1}$$

where ϵ is the electric permittivity, N the number of units of differential capacitors, A and d_0 the overlap area and initial gap between the movable beam and each stationary beam, respectively. $f=0.65 d_0/h$ is the fringing field correction factor, where h is the beam height.¹⁴

Displacement of the movable beams is equal to the deflection of the folded beams in the transverse direction. The displacement results in a capacitance changes ΔC given by

$$\Delta C = C_1 - C_2 = N\epsilon A \left(\frac{1}{d_0 - \Delta d} - \frac{1}{d_0 + \Delta d} \right) \approx \frac{2N\epsilon A}{d_0^2} \Delta d, \tag{2}$$

where Δd is the displacement of the load sensor. The fringing effect factor is cancelled out. When Δd is within 50% of the initial gap, the capacitance change is approximately linearly proportional to the sensor displacement. This large linear range is one of the advantages of differential capacitance sensing over direct capacitance sensing.

There are a number of methods to measure changes in capacitance. Figure 1(d) shows the schematic of the charge sensing method. This method can effectively mitigate the effect of parasitic capacitances, which generally exist in electrostatic MEMS devices. Two complementary high-

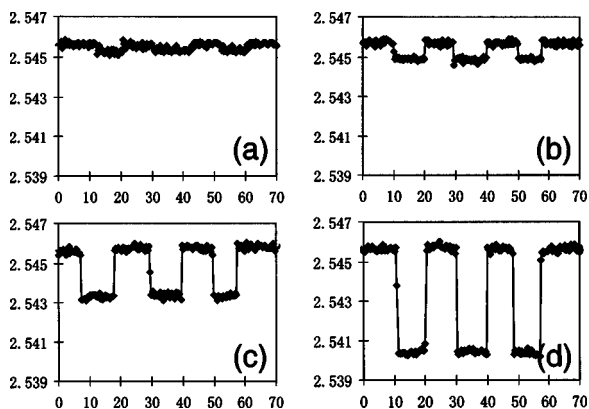


FIG. 3. Recorded raw data of output voltage V_{sense} at (a) 1 V, (b) 2.5 V, (c) 4 V, and (d) 5.5 V actuation voltages. Horizontal axis is time and vertical axis is output voltage V_{sense} .

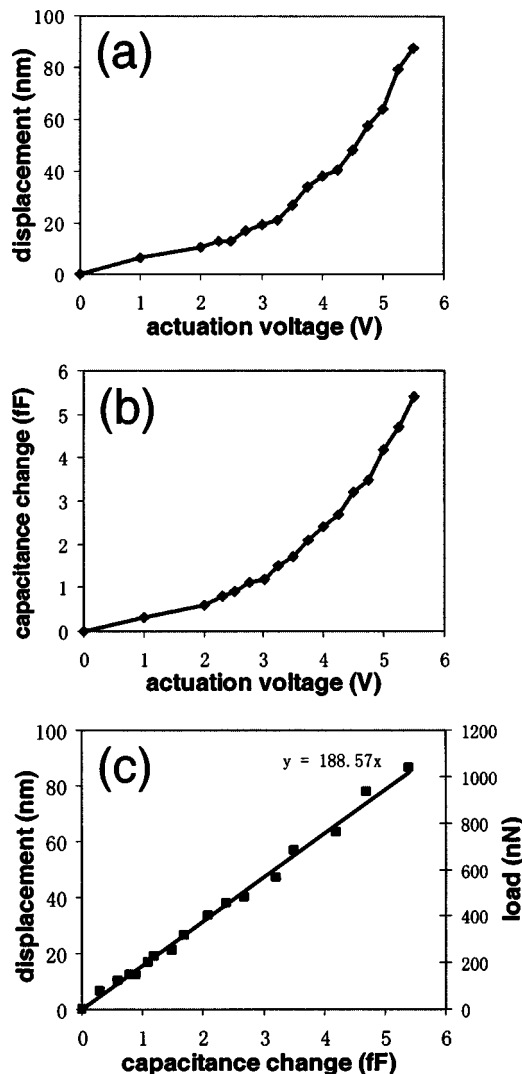


FIG. 4. (a) Displacements of the load sensor obtained from image analysis at different actuation voltages; (b) capacitance change at different actuation voltages; (c) calibration of both displacement and load as a function of measured capacitance change of the load sensor for testing CNTs (stiffness is 11.8 N/m). The fitting straight line is for the load.

frequency alternate current (ac) signals are applied to each set of the stationary beams of the load sensor, and the sensing output is an ac signal which measures the capacitance change ΔC . This output is amplified, synchronously demodulated, and low-pass filtered to give a direct current (dc) output signal.¹⁵ In brief, change of the dc voltage V_{sense} is proportional to the capacitance change;

$$\Delta V_{sense} = \frac{V_0}{C_f} \Delta C, \tag{3}$$

where ΔV_{sense} is the change of output voltage, V_0 the amplitude of ac voltage applied to the stationary beams, and C_f the feedback capacitor.¹⁵

A commercial integrated circuit (IC) based on the principle discussed above (Universal Capacitive Readout MS3110, Microsensors, Inc.) was used in the measurement. The MEMS device chip was positioned very close to the sensing IC chip (MS3110) in order to minimize the stray capacitance and electromagnetic interference. This was accomplished by placing both chips on a custom-made printed circuit board with grounded shields on both sides.

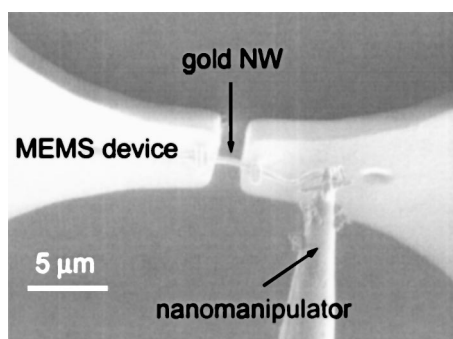


FIG. 5. Gold NW was positioned across the gap between the actuator and the load sensor. Specimen ends were fixed by electron beam induced deposition (EBID) (Refs. 5 and 6) of platinum.

In order to calibrate the displacement obtained by capacitance measurement, an otherwise identical device without gap was fabricated on the same chip. Real time high resolution images were employed to calibrate the capacitance measurements.¹⁶ The calibration process was done inside a field emission SEM (Leo Gemini 1525). The device was actuated at a series of stepwise increasing voltages, applied sequentially in six ON-OFF cycles. A high contrast feature on the movable shuttle was selected for capturing images at high magnification ($\times 183k$). The device corresponding to the ON-OFF actuation cycles was captured in one SEM image, as shown in Fig. 2. Simultaneously, the output voltage V_{sense} was recorded by a digital multimeter and converted to capacitance change using Eq. (3). Figure 3 shows the raw data of V_{sense} at several actuation voltages (1, 2.5, 4, and 5.5 V).

The images were analyzed to identify displacements with the following procedure: the line-by-line scanning was transformed to an intensity matrix of 1024×768 pixels. To correlate the OFF-ON images, two polynomial functions were used to fit the intensity distribution for the last scanned line corresponding to OFF, $f(x)$, and for the first scanned line corresponding to ON, $g(x)$, respectively. These two functions were interpolated to subpixel level and the shift, u , was obtained by finding the best match between functions $f(x)$ and $g(x+u)$. The iterative process was stopped when $\int_{\Omega} [g(x+u) - f(x)]^2 dx$ was smaller than a prescribed tolerance. The domain Ω was defined to span the feature in the movable shuttle. Using the calibration factor of the SEM image at the corresponding scale, we converted the shift u in pixels to displacement (nm). Note that this image analysis has the advantage of eliminating the influence of drift, which typically accumulates with time, and results in sub-pixel resolution.

Figure 4(a) shows the displacement of the load sensor as a function of actuation voltage. Figure 4(b) shows the measured capacitance change as a function of actuation voltage. C_f was selected so that 1 mV change of V_{sense} corresponded to 1 fF change of capacitance. Figure 4(c) correlates the displacement/load and the capacitance change. It follows a linear relationship, which agrees with Eq. (2). The achievable resolution of the measured capacitance change is 0.2 fF, and the corresponding displacement resolution is 3 nm.

Another important step in the calibration procedure is the accurate measurement of the load sensor stiffness. This can be accomplished in one of two ways: (i) by resonating the structure, a common procedure in MEMS research,¹⁰ or (ii) by identifying the Young's modulus of the material, E ,

and then using finite element analysis (FEA) with accurate metrology. In view that for the parallel beams in the load sensor the resonating voltage is larger than the *pull-in* voltage, the second methodology was employed. Its accuracy was assessed by determining the comb-drive actuator stiffness using the resonance method and then by comparing this result with the one calculated using FEA. In the resonance method the stiffness is calculated from $K = (2\pi f_r)^2 (M_s + 0.3714M_b)$,¹⁰ where f_r is the resonant frequency, M_s and M_b the masses of the shuttle and the folded beams, respectively. For the comb-drive actuator shown in Fig. 1(b), we measured a resonant frequency of 17.2 ± 0.1 kHz. The corresponding stiffness is 20.3 N/m, while the computed stiffness based on the *measured* folded beam geometry, using $E = 170$ GPa,¹⁷ was 20.7 N/m. This clearly shows that the stiffness computed based on the fabricated geometry and the known value of Young's modulus is in good agreement with that identified from the resonance experiment. Following this procedure, the stiffness of the load sensor designed for the testing CNTs was computed to be 11.8 N/m, which corresponds to a load resolution of 35 nN.¹⁸ Likewise, the stiffness of the load sensor designed for testing NWs was 48.5 N/m with a load resolution of 145 nN.

Gold NWs and amorphous CNTs have been mounted on the device across the gap using a nanomanipulator from Klocke Nanotechnik, see Fig. 5. *In situ* testing of nanostructures is being pursued and will be reported in future publications.

This project is supported by the National Science Foundation under Award No. DMR-0315561. Nanomanipulation was carried out in the Center for Microanalysis of Materials, University of Illinois, which is partially supported by the U.S. Department of Energy under Grant No. DEFG02-96-ER45439.

¹M. M. J. Treacy, T. W. Ebbesen, and J. M. Gibson, *Nature (London)* **381**, 678 (1996).

²P. Poncharal, Z. L. Wang, D. Ugarte, and W. A. de Heer, *Science* **283**, 1513 (1999).

³M. R. Falvo, G. J. Clary, R. M. Taylor, V. Chi, F. P. Brooks, S. Washburn, and R. Superfine, *Nature (London)* **389**, 582 (1997).

⁴E. W. Wong, P. E. Sheehan, and C. M. Lieber, *Science* **277**, 1971 (1997).

⁵M. F. Yu, O. Lourie, M. J. Dyer, K. Moloni, T. F. Kelly, and R. S. Ruoff, *Science* **287**, 637 (2000).

⁶P. A. Williams *et al.*, *Appl. Phys. Lett.* **80**, 2574 (2002).

⁷M. A. Haque and M. T. A. Saif, *Sens. Actuators, A* **97-98**, 239 (2002).

⁸S. Lu, D. A. Dikin, S. Zhang, F. T. Fisher, J. Lee, and R. S. Ruoff, *Rev. Sci. Instrum.* **75**, 2154 (2004).

⁹L. Que, J. S. Park, and Y. B. Gianchandani, *J. Microelectromech. Syst.* **10**, 247 (2001).

¹⁰W. C. Tang, T. H. Nguyen, M. W. Judy, and R. T. Howe, *Sens. Actuators, A* **21-23**, 328 (1990).

¹¹H. D. Espinosa, Y. Zhu, and B. Peng, *2002 Annual Meeting of the Society of Experimental Mechanics*, Milwaukee, WI, 10-12 June 2002.

¹²B. C. Prorok, Y. Zhu, H. D. Espinosa, Z. Guo, Z. P. Bazant, Y. Zhao and B. I. Yakobson, in *Encyclopedia of Nanoscience and Nanotechnology*, edited by H. S. Nalwa (American Scientific, Stevenson Ranch, CA, 2004), Vol. 5, pp. 555-600.

¹³Y. Zhu and H. D. Espinosa, *J. Microelectromech. Syst.* (submitted).

¹⁴J. M. Huang, K. M. Liew, C. H. Wong, S. Rajendran, M. J. Tan, and A. Q. Liu, *Sens. Actuators, A* **93**, 273 (2001).

¹⁵S. D. Senturia, *Microsystem Design* (Kluwer Academic, Boston, 2002).

¹⁶C. Q. Davis and D. M. Freeman, *Opt. Eng.* **37**, 1299 (1998).

¹⁷W. N. Sharpe, Jr., B. Yuan, and R. Vaidyanathan, *Proceedings of the Tenth IEEE International Workshop on MEMS*, Nagoya, Japan, 1997.

¹⁸The failure force of multiwalled CNTs was reported ranging from 400 to 1340 nN.⁵